Numerical simulation of wake effects in the lee of a farm of Wave Dragon wave energy converters

C. Beels[1], P. Troch[1], K. De Visch[1], G. De Backer[1], J. De Rouck[1] and J.P. Kofoed[2]

[1]Department of Civil Engineering,
Ghent University,
Technologiepark 904, 9052 Zwijnaarde, Belgium
E-mail: charlotte.beels@ugent.be

[2]Department of Civil Engineering,
Aalborg University,
Sohngaardsholmsvej 57, 9000 Aalborg, Denmark
E-mail: jpk@civil.aau.dk

Abstract

The contribution of wave energy to the renewable energy supply is rising. To extract a considerable amount of wave power, Wave Energy Converters (WECs) are arranged in several rows or in a 'farm'. The wake behind each individual WEC in the farm affects the power absorption of its neighbouring WECs.

In this paper wake effects in the lee of a single Wave Dragon WEC and multiple Wave Dragon WECs are studied in a time-dependent mild-slope equation model. The Wave Dragon WEC is a floating offshore converter of the overtopping type. The water volume of overtopped waves is first captured in a basin above mean sea level and then drains back to the sea through hydro turbines.

The wake dimensions behind a single Wave Dragon WEC are investigated for uni- and multidirectional waves. An increasing directional spreading results in a faster wave redistribution behind the WEC. The power absorption of a farm of five Wave Dragon WECs, installed in a staggered grid, is calculated for varying in-between distances. It is observed that an in-between distance of 2D is preferred, when taking spatial and safety considerations into account.

Keywords: farm, mild-slope equation, wake, wave energy

Nomenclature

f	=	wave frequency [Hz]
g	=	gravitational acceleration [m/s^2]
h	=	water depth [m]
k	=	wave number [rad/m] = $\frac{2\pi}{L}$
l	=	longitudinal spacing [m]
p	=	wave power [W/m]
s	=	directional spreading parameter [-]
t	=	time [s]
w	=	lateral spacing [m]
C	=	phase velocity [m/s] = $\frac{L}{T}$
C_g	=	group velocity [m/s] = $\frac{C}{2}\left(1+\frac{2kh}{\sinh(2kh)}\right)$
D	=	distance between the tips of the wave reflectors [m]
H_s	=	significant wave height [m]
K_d	=	disturbance coefficient [-]
L	=	wave length [m]
P	=	wave power [W]
R_c	=	crest freeboard [m]
T	=	wave period [s]
W	=	width [m]
η	=	surface elevation [m]
θ	=	angle of wave ray from x-axis [°]
θ_0	=	mean wave angle from x-axis [°]
λ_{d_B}	=	ratio between the time averaged amount of energy flux, integrated from the draft of the main body up to the surface, and the time averaged amount of incident energy flux, integrated from the seabed up to the surface [-]
ϕ	=	velocity potential [m^2/s]
ρ	=	density of sea water [kg/m^3]
ω	=	angular frequency [rad/s] = $2\pi f$
Δt	=	time step [s]
Δx	=	grid size in x-direction [m]
Δy	=	grid size in y-direction [m]
$D(f,\theta)$	=	directional spreading function [1/°]
∇	=	horizontal gradient operator

Subscripts

p	=	peak value
max	=	maximum value
min	=	minimum value
a	=	absorbed
i	=	incident
r	=	reflected
t	=	transmitted
d	=	disturbed

cs	=	cross section
R	=	reflector
B	=	main body

Superscripts

$^-$	=	value for carrier frequency

1 Introduction

The increasing energy demand and the Kyoto agreement to reduce the greenhouse gasses, have renewed the interest in renewable energy. In the past 10 years many concepts for wave power conversion have intensively been studied and developed, a.o. the Wave Dragon Wave Energy Converter (WEC) [1]. The Wave Dragon WEC is a floating offshore WEC of the overtopping type with a rated power of 4 MW in a 24 kW/m wave climate. The Wave Dragon WEC consists of two main structural elements (Fig. 1):

- two wave reflectors to focus the incident waves towards a ramp;
- a main body where the focussed waves run up the curved ramp, overtop in a water reservoir above mean sea level and consequently have an increased potential energy compared to the surrounding sea. The obtained potential energy is converted into electricity when the stored water drains back to the sea through hydro turbines.

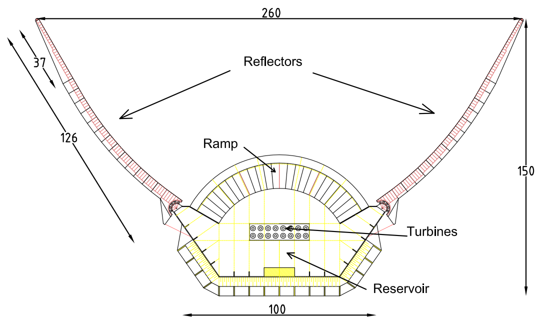

Figure 1: Main structural elements of a Wave Dragon WEC in plan view (copyright Wave Dragon) - dimensions in m

To produce amounts of power comparable to a classic power plant, several Wave Dragon WECs need to be installed in a geometric configuration or in a 'farm'. Wave Dragon WECs in a farm are partly absorbing, partly redistributing the incident wave power. Consequently the power absorption of each individual Wave Dragon WEC in a farm is affected by its neighbouring Wave Dragon WECs. The wave climate around each Wave Dragon WEC determines its performance in the farm.

In this paper the wake in the lee of a single Wave Dragon WEC and multiple Wave Dragon WECs is studied in a phase-resolving time domain model based on the mild-slope equations, MILDwave, developed at Ghent University [2].

The wave reflectors and the main body (ramp and reservoir) of the Wave Dragon WEC are simulated as porous structures, with similar reflection, respectively absorption, characteristics as obtained for the prototype Wave Dragon WEC by using the sponge layer technique [2]. A detailed description of the implementation of a Wave Dragon WEC in MILDwave is provided in [3].

In the next section the basic equations for wave generation and wave propagation in MILDwave are briefly described. Furthermore the implementation of a Wave Dragon WEC in MILDwave through the sponge layer technique is discussed. The wake behind a single Wave Dragon WEC is studied in detail for uni- and multidirectional waves with varying directional spreading in section 3. In the last section the power absorption of a farm of five Wave Dragon WECs installed in a staggered grid is estimated for varying in-between distances between the Wave Dragon WECs.

2 Mild-slope wave propagation model MILDwave

2.1 Wave generation and propagation

The mild-slope equations of Radder and Dingemans (1985) [4], which describe the transformation of linear irregular waves with a narrow frequency band over a mildly varying bathymetry (bed steepness up to 1/3 [5]) are given in Eqn. (1) and Eqn. (2):

$$\frac{\partial \eta}{\partial t} = B\phi - \nabla \cdot (A \nabla \phi) \quad (1)$$

$$\frac{\partial \phi}{\partial t} = -g\eta \quad (2)$$

where η and ϕ are the surface elevation and velocity potential at the free water surface, respectively, ∇ is the horizontal gradient operator, t is the time, g is the gravitational acceleration and where the value of A and B is calculated with Eqn. (3) and Eqn. (4):

$$B = \frac{\overline{\omega}^2 - \overline{k}^2 \overline{C}\overline{C_g}}{g} \quad (3)$$

$$A = \frac{\overline{C}\overline{C_g}}{g} \quad (4)$$

with the phase velocity $\overline{C}$ and the group velocity $\overline{C_g}$ for a wave with carrier wave number $\overline{k}$ $\left(= \frac{2\pi}{\overline{L}}\right)$, carrier angular frequency $\overline{\omega}$ $\left(= 2\pi\overline{f}\right)$, carrier wave length $\overline{L}$ and carrier frequency $\overline{f}$. Overbar ($^-$) denotes that the wave characteristic is calculated for the carrier frequency.

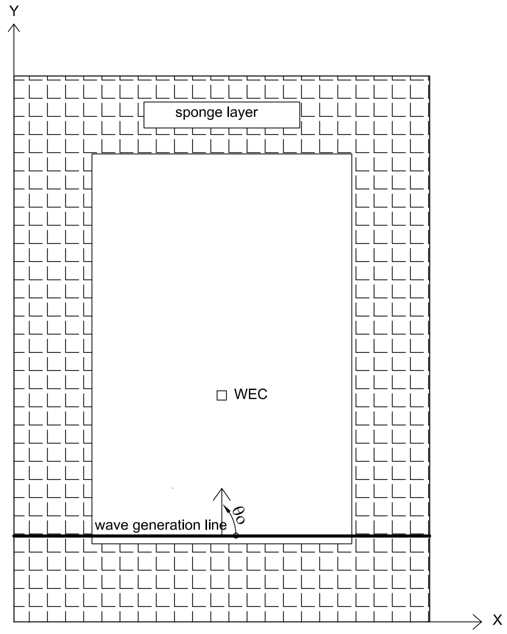

Figure 2: Definition sketch of wave basin in plan view for generation of unidirectional waves

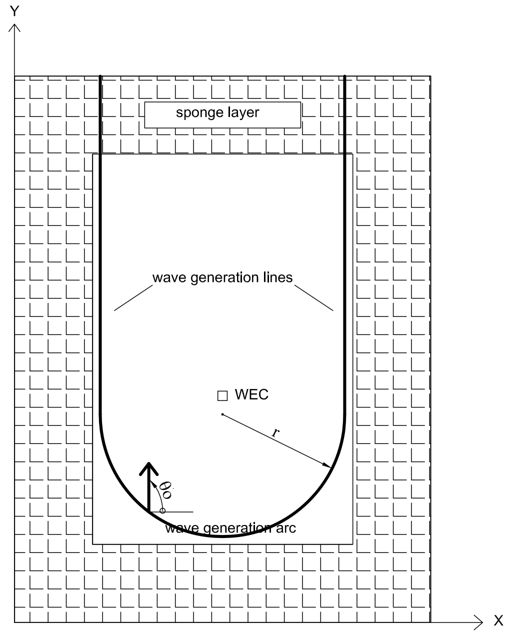

Figure 3: Definition sketch of wave basin in plan view for generation of multidirectional waves

In MILDwave waves are generated at the offshore boundary (Fig. 2) by using the source term addition method, i.e. by adding an additional surface elevation to the calculated value on a wave generation line for each time step [6]. The wave generation line is assumed to be parallel to the x-axis in Fig. 2.

It has been proven that the model of Radder and Dingemans (1985) can be used to simulate the transformation of uni- and multidirectional random waves [6]. To generate unidirectional irregular waves a parameterised JONSWAP spectrum has been used as an input spectrum [7]. The set-up in Fig. 2 cannot be applied for the generation of multidirectional irregular waves as not all components of these waves are travelling in the same direction.

Recently, Lee and Yoon (2007) [8] developed a method for internally generating multidirectional waves on an arc in a rectangular grid system using the source term addition method (Fig. 3). The grid point nearest to the arc is used as a wave generation point.

Eqn. (5) gives the directional spreading function $D(f,\theta)$ to generate short-crested waves [9]:

$$D(f,\theta) = \frac{2^{2s-1}}{\pi}\frac{\Gamma^2(s+1)}{\Gamma(2s+1)}\cos^{2s}\left(\frac{\theta-\theta_o}{2}\right) \quad (5)$$

with the angle of wave rays from the x-axis θ ($0^\circ \leq \theta \leq 360^\circ$) and the mean wave angle θ_o. The directional spreading parameter s gives the degree of directional energy concentration. The parameter s can be related to the frequency by Eqn. (6) [10]:

$$s = \begin{cases} (f/f_p)^5 s_{max} & : \quad f \leq f_p \\ (f/f_p)^{-2.5} s_{max} & : \quad f \geq f_p \end{cases} \quad (6)$$

with the peak wave frequency f_p. The parameter s_{max} is the maximum value of the spreading parameter and is equal to 10, 25 and 75 for wind waves, swell waves with a short decay distance and swell waves with a long decay distance, respectively [10].

The effect of the fully reflective domain boundaries is negligible because absorbing sponge layers [11] at the outside boundaries (Fig. 2 and Fig. 3) are significantly dissipating the incoming wave energy by multiplying the calculated surface elevations on each new time step with an absorption function. In general, a length of $2.5L_{max}$ [6], where L_{max} is the maximum wave length resulting from the cut-off incident frequency spectrum, is sufficient.

A finite difference scheme, as described in [12], is used to solve Eqn. (1) and Eqn. (2). The domain is divided in grid cells (uniform grid) with dimensions Δx and Δy and central differences are used for spatial as well as time derivates. The grid spacing $\Delta x = \Delta y$ is chosen so that $\frac{L_{min}}{20} \leq \Delta x = \Delta y \leq \frac{L_{min}}{10}$ (L_{min} = shortest wave length (maximum frequency) for irregular waves) and the time step meets the Courant-Friedrichs-Lewy criterion, $\Delta t \leq \frac{\Delta x}{C}$, to guarantee a stable and consistent result.

Wave generation starts from quiescent water conditions at $t = 0$. A slow start of wave generation is obtained by multiplying the wave generation by $\tanh\left(\frac{0.5t}{T}\right)$ [13], with the wave period T. Each time step, η and ϕ are calculated in the centre of each grid cell. Consequently, waves are gradually propagating through the domain.

2.2 Implementation of a Wave Dragon WEC in MILDwave

In this paper a Wave Dragon WEC with an installed power of 4 MW, in a typical wave climate of the northern part of the North Sea (24 kW/m), is studied. The dimensions of the Wave Dragon WEC are shown in Fig. 1. Wave situations in the northern part of the North Sea [14] for significant wave heights between 0.5 and 5.5 m and their related wave power (assuming a parameterized JONSWAP spectrum with $\gamma = 3.3$ and deep water) and frequency of occurrence are given in Table 1. During the rest of the year (frequency of occurrence = 10 %), wave heights are mainly smaller than 0.5 m and sometimes larger than 5.5 m. These situations are neglected in the following, as they contribute only marginally to the total power production over a year. The mean wave power of the 5 considered wave situations is approximately 16 kW/m. Waves with a significant wave height H_s = 1 m and peak wave period T_p = 5.6 s have the highest frequency of occurrence (43 %).

Table 1: Wave situations in the northern part of the North Sea (Location Ekofisk: distance to shore = 300 km, water depth = 71 m [14])

Wave situation $[-]$	H_s $[m]$	T_p $[s]$	Incident wave power p_i $[kW/m]$	Frequency of occurrence $[\%]$
1	1	5.6	2.5	43
2	2	7.0	12.4	25
3	3	8.4	33.5	12
4	4	9.8	69.6	6
5	5	11.2	124.2	4

A Wave Dragon WEC, installed in sea, is interacting with the incoming waves. The incident waves are partly overtopped in the reservoir and consequently absorbed. The other part is reflected on the WEC or transmitted under the WEC or diffracted around the structure. Therefore the Wave Dragon WEC is only absorbing a certain amount of the incident wave power available over the width of the device.

The Wave Dragon WEC consists of 2 main structural elements with a different functioning (Fig. 4): (i) wave reflectors (subscript R) which reflect part of the incident wave power $p_{R,r}$ towards the main body and (ii) a main body (subscript B) which is absorbing as much wave power as possible $P_{cs,B,a}$. The wave reflectors partly reflect the incident wave power p_i to increase the available wave power in front of the main body. The remaining incident wave power (i.e. not reflected part) is transmitted under the wave reflectors $p_{R,t}$. The increased wave power in front of the main body $P_{cs,R,i}$ is not completely absorbed by the main body, but is partly lost by transmission under the main body $P_{cs,B,t}$ and by reflection on the curved ramp $P_{cs,B,r}$.

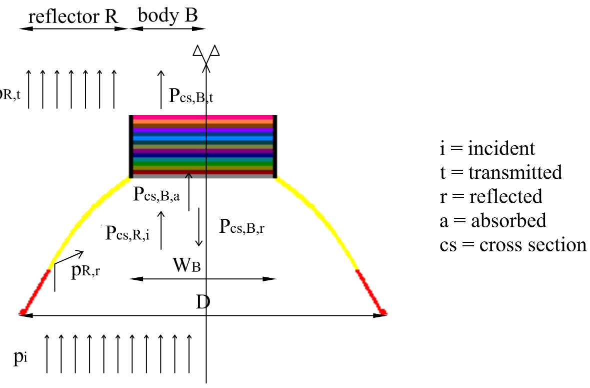

Figure 4: Definition sketch of reflection on and transmission under the wave reflector and reflection on, transmission under and absorption by the main body - plan view

Therefore the implementation of a Wave Dragon WEC in MILDwave is carried out in two phases: implementation of (i) wave reflectors and (ii) main body. The implementation of a Wave Dragon WEC in MILDwave is explained in detail in [3]. In this section a short summary is given.

The wave reflectors have been implemented as porous structures (covering the spatial dimensions of the wave reflectors) with a given degree of reflection and transmission. The efficiency (amount of reflection) of the wave reflectors has been determined in [15]. The efficiency increases for waves with a higher wave frequency. The transmission under the wave reflectors has been derived by assuming that all wave power below the draft of the wave reflectors is transmitted, $p_{R,t}$. The transmission increases for increasing wave period. As the amounts of reflection on and transmission below the wave reflectors are known, the wave reflectors can be tuned in MILDwave with the sponge layer technique.

The main body has been implemented as an array of cells (covering the spatial dimensions of the main body) that have been assigned a given degree of absorption by using the sponge layer technique. By changing the values of the absorption coefficients, the degree of reflection and transmission and consequently absorption of the porous structure (main body) can be tuned. The absorption of the main body $P_{cs,B,a}$ has been derived by estimating the overtopping rate and is given by equation (7) [16, 17]:

$$P_{cs,B,a} = 0.4\exp^{-3.2\frac{R_c}{H_s}} \lambda_{d_B} \sqrt{gH_s^3} R_c g \rho W_B \qquad (7)$$

with the crest freeboard R_c, the significant wave height H_s, the ratio between the time averaged amount of energy flux integrated from the draft of the main body up to the surface and the time averaged amount of incident energy flux integrated from the seabed up to the surface, λ_{d_B}, the density of sea water, ρ, and the width of the ramp W_B.

Not all wave power in the cross section in front of the main body $P_{cs,R,i}$ is absorbed by the main body. It is again assumed that all wave power below the draft of the main body is transmitted ($P_{cs,B,t}$). The remaining wave power $P_{cs,B,r}$ is reflected. The amount of reflection is decreasing with increasing wave period while the amount of transmission is increasing. The determined values of $P_{cs,B,a}$, $P_{cs,R,i}$, $P_{cs,B,t}$ and $P_{cs,B,r}$ have been used to implement the main body in MILDwave with the sponge layer technique.

3 Wake behind a single Wave Dragon WEC

By assembling both structural elements (reflectors and main body) a Wave Dragon WEC is implemented in a wave basin in MILDwave, as shown in Fig. 6. As the Wave Dragon WEC is floating, the WEC will move and may disturb the wave pattern. However, open air-chambers under the main body with a pressurized air system are not only adjusting the floating height, but are also reducing the movements of the Wave Dragon WEC. Furthermore its size makes the Wave Dragon WEC more stable. In this paper the Wave Dragon WEC is assumed to be restrained and consequently movements are neglected.

In this section the wake behind a single Wave Dragon WEC has been studied for the wave situation with the highest frequency of occurrence (Table 1), i.e. H_s = 1 m and T_p = 5.6 s. In section 4 wave situation 3 (H_s = 3 m and T_p = 8.4 s) will be considered as well.

For the generation of irregular long-crested waves (500 waves) 50 frequency components are used. The number of frequency components is reduced to 20 to generate short-crested waves (1000 waves) with a time step of 0.1 s and 0.05 s for T_p = 5.6 s and T_p = 8.4 s, respectively (cell dimensions of 1 m for both wave periods). A uniform deep water depth h (= 200 m) is used to avoid energy dissipation due to bottom friction and wave breaking.

The disturbance coefficients K_d in a wave basin with a single Wave Dragon WEC for long-crested (head on) waves with a significant wave height of 1 m and a peak wave period of 5.6 s are shown in Fig. 6(a). The disturbance coefficient $K_d = \left(\frac{H_{s,d}}{H_{s,i}}\right)$ is defined as the ratio between the numerically calculated disturbed significant wave height, $H_{s,d}$, and the numerically calculated incident significant wave height at the wave generation boundary, $H_{s,i}$. Only the useful domain without sponge layers is shown. The Wave Dragon WEC is indicated in black. Immediately behind the Wave Dragon WEC a large decrease of the significant wave height is seen, while a gradual redistribution occurs behind the Wave Dragon WEC due to diffraction around the WEC. The large wave height decrease right behind the Wave Dragon WEC does not imply that all energy is absorbed. For irregular long-crested waves with H_s = 1 m and T_p = 5.6 s approximately 70 % of the wave power in front of the main body $P_{cs,R,i}$ is reflected (28 % is absorbed and 0.02 % is transmitted [3]).

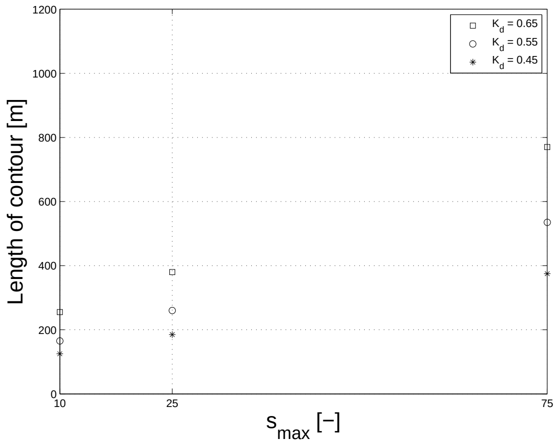

Figure 5: Length of wake (K_d contour = 0.65, 0.55 and 0.45) for irregular short-crested waves with T_p = 5.6 s and s_{max} = 75, 25 and 10

In the following the power absorption of a single Wave Dragon WEC in the considered wave climate is denoted by U. A second Wave Dragon WEC installed right behind the first one at y = 1 750 m, and 3 750 m in only absorbing $P_{cs,B,a}$ = 0.12 U and 0.29 U (Eqn. (7)), respectively, as the average available wave power p_i in those sections is 18 % and 37 %, respectively, of the available wave power p_i = 2.48 kW/m in front of the first WEC. For this long-crested wave condition, a very large distance between the WECs is needed to have a sufficient wave height behind the first WEC. One should keep in mind that so far only long-crested (no directional spreading) incident waves with T_p = 5.6 s have been considered. The wake behind a single Wave Dragon WEC in a short-crested sea with a mean wave direction of 90° and a directional spreading of approximately 9° (s_{max} = 75), 16° (s_{max} = 25) and 24° (s_{max} = 10) for the peak period (T_p = 5.6 s) is shown in Fig. 6(b), Fig. 6(c) and Fig. 6(d), respectively.

As expected, the wake length shortens with increasing directional spreading due to a faster redistribution behind the WEC. A wider wake is observed when short-crested waves are generated. Furthermore, the small increase in wave height, as seen at the edges of the wake in Fig. 6(a), disappears in a short-crested sea. The length of the wake as a function of directional spreading is shown in Fig. 5 for three K_d contours (K_d = 0.65, 0.55 and 0.45). For higher values of K_d it is rather difficult to define the length of the contour as the contour is less well-defined. The wake in short-crested waves with s_{max} = 25 is approximately 1.5 times longer compared to the wake in short-crested waves with s_{max} = 10. For short-crested waves with the smallest directional spreading (s_{max} = 75) the wake length is approximately 3 times the wake length observed in a short-crested sea with s_{max} = 10.

Three lateral sections S1, S2 and S3 behind the Wave Dragon WEC (indicated on Fig. 6) are shown in Fig. 7 for the same wave conditions as considered in Fig. 6. The wave height decrease right behind the Wave Dragon WEC at y = 750 m is comparable for the four wave conditions.

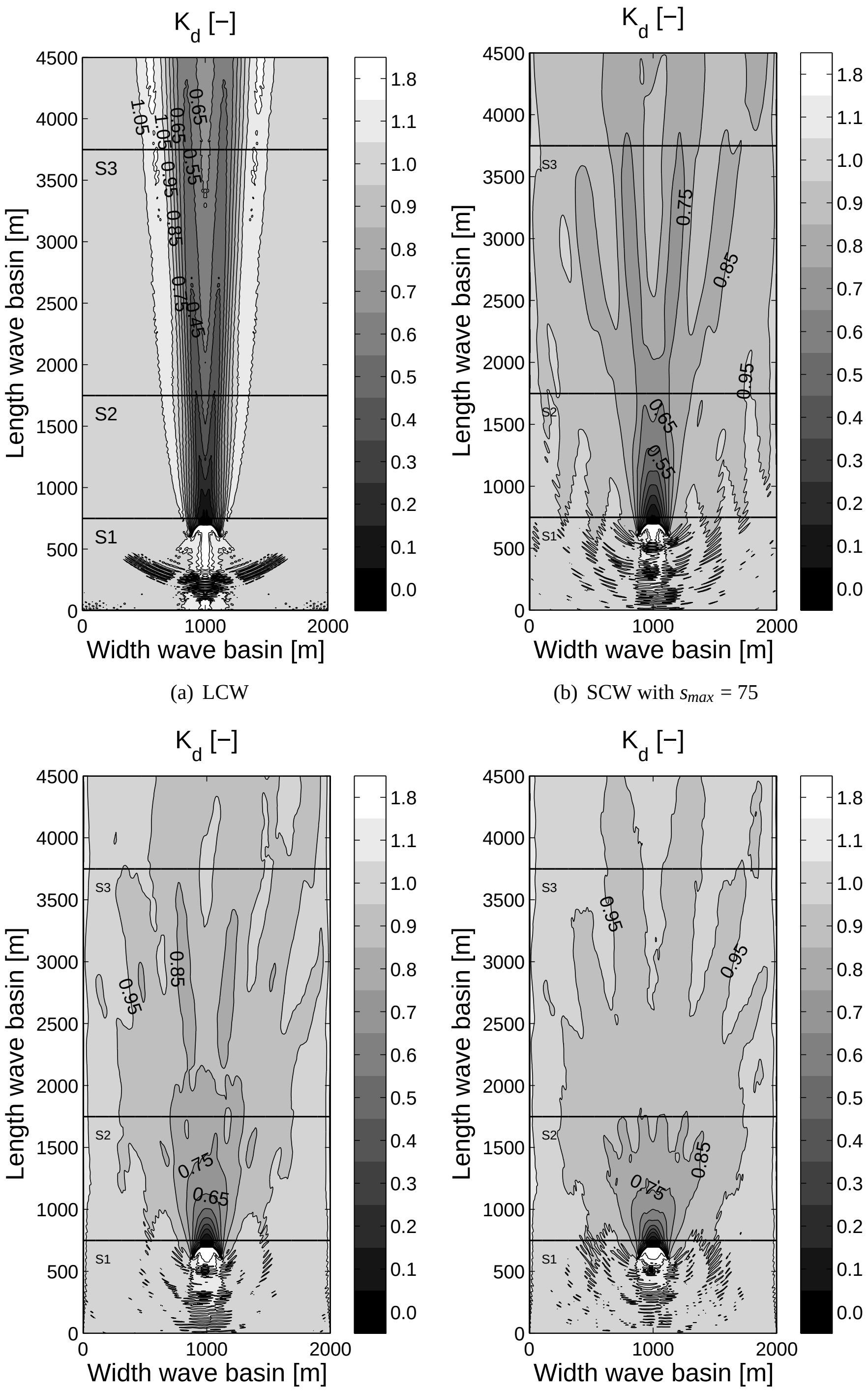

(a) LCW

(b) SCW with s_{max} = 75

(c) SCW with s_{max} = 25

(d) SCW with s_{max} = 10

Figure 6: Calculated disturbance coefficient K_d in a wave basin with a single Wave Dragon WEC for irregular (a) long-crested waves (head on) with T_p = 5.6 s and short-crested waves (head on) with T_p = 5.6 s and s_{max} = (b) 75, (c) 25 and (d) 10

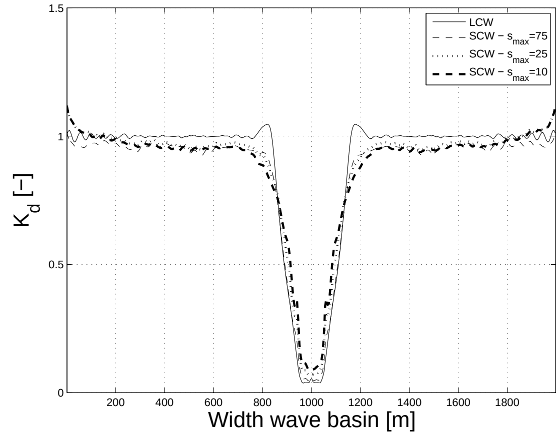

(a) Section S1 at y = 750 m

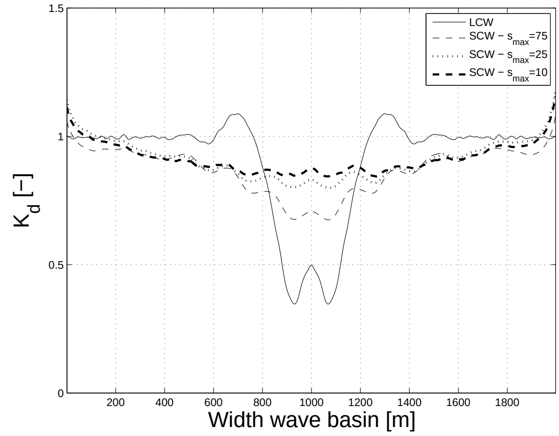

(b) Section S2 at y = 1 750 m

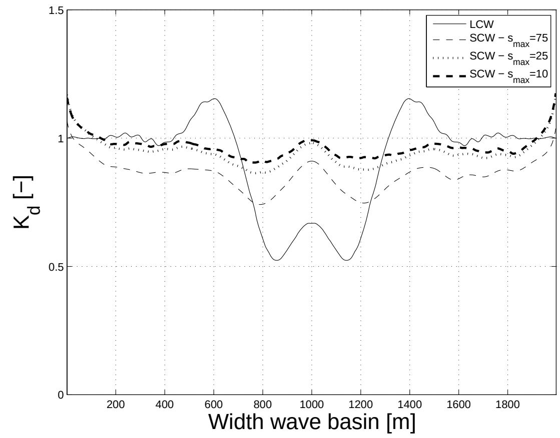

(c) Section S3 at y = 3 750 m

Figure 7: Calculated disturbance coefficient K_d in lateral cross sections at y = (a) 750 m, (b) 1 750 m and (c) 3 750 m, as indicated on Fig. 6, in a wave basin with a single Wave Dragon WEC for irregular long-crested waves (LCW) with T_p = 5.6 s and short-crested waves (SCW) with T_p = 5.6 s and s_{max} = 75, 25 and 10

At y = 1 750 m the effects of the directional spreading are clearly present. The remaining wave height behind the Wave Dragon WEC increases with increasing directional spreading.

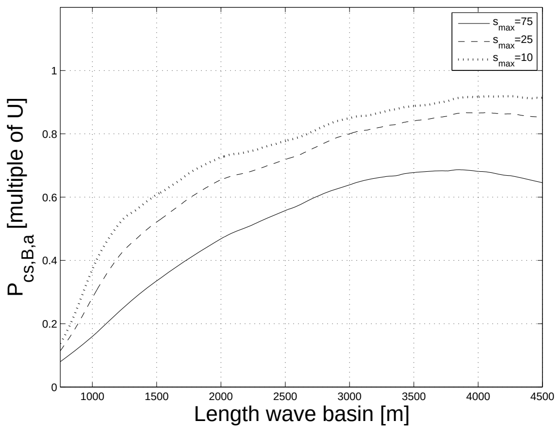

(a) WEC installed between x = 870 m and x = 1130 m

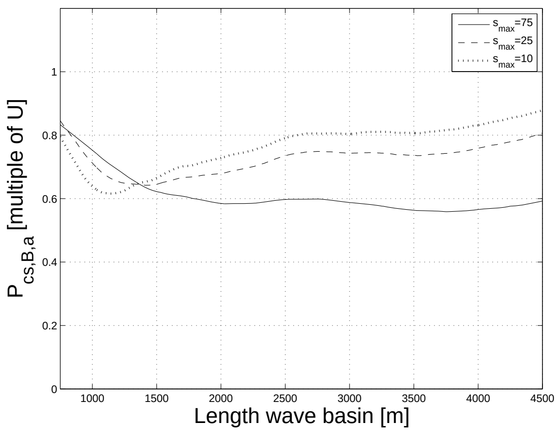

(b) WEC installed between x = 610 m and x = 870 m

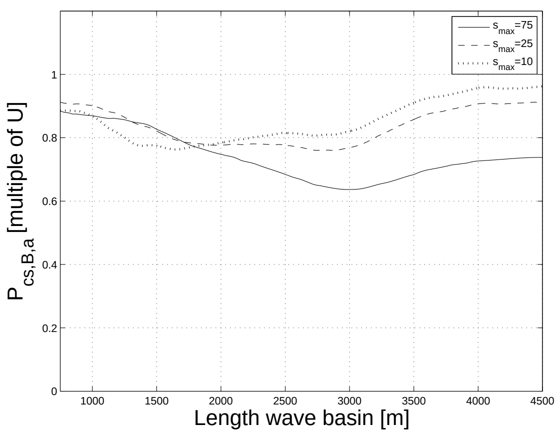

(c) WEC installed between x = 350 m and x = 610 m

Figure 8: Power absorption of a second Wave Dragon WEC installed between (a) x = 870 m and x = 1130 m, (b) x = 610 m and x = 870 m and (c) x = 350 m and x = 610 m, in a wave basin with a single Wave Dragon WEC for irregular short-crested waves (SCW) with T_p = 5.6 s and s_{max} = 75, 25 and 10

At y = 3 750 m (3 km behind the WEC) the wave height is practically equal to the wave height in front of the WEC for short-crested waves with $s_{max} = 10$. A Wave Dragon WEC installed right behind the first one at y = 1 750 m and 3 750 is absorbing $P_{cs,B,a}$ = 0.41 U and 0.68 U (Eqn. (7)), respectively, when s_{max} = 75, $P_{cs,B,a}$ = 0.6 U and 0.86 U (Eqn. (7)), respectively, when

$s_{max} = 25$ and $P_{cs,B,a}$ = 0.67 U and 0.9 U (Eqn. (7)), respectively, when $s_{max} = 10$.

So far the potential power absorption right behind a single Wave Dragon WEC has been studied. In Fig. 8 the potential power absorption of a second Wave Dragon WEC installed right behind the first Wave Dragon WEC is compared to the potential power absorption of a second Wave Dragon WEC shifted over 260 m (WEC installed between x = 610 m and x = 870 m) and 520 m (WEC installed between x = 350 m and x = 610 m). The potential power absorption (Eqn. (7)) of a second Wave Dragon WEC installed between x = 870 m and x = 1130 m, between x = 610 m and x = 870 m and between x = 350 m and x = 610 m, along the length of the wave basin is shown in Fig. 8 for irregular short-crested waves with T_p = 5.6 s and s_{max} = 75, 25 and 10. Note that these values are only given behind the first Wave Dragon WEC.

The potential power absorption between y = 750 m and y = 2500 m is higher further away from the first WEC, e.g. the potential power absorption at y = 1250 m is increasing from approximately 0.55 U for a Wave Dragon WEC installed between x = 870 m and 1130 m to 0.8 U for installation between x = 350 m and x = 610 m.

For a Wave Dragon WEC installed between x = 610 m and x = 870 m and between x = 350 m and x = 610 m, the potential power absorption is first decreasing and afterwards increasing, as there is no influence of the wake in the beginning. The initial wave height decrease is higher for s_{max} = 10 as the wake is wider compared to s_{max} = 25.

In the case of long-crested waves and swell waves (with s_{max} = 75) a second WEC installed 3 km behind the first WEC is absorbing less than 70 % of the first WEC. As in practice the available space to install a farm of WECs is rather small, a WEC in a second row should not be installed right behind a WEC in the first row. Therefore, in the next section a farm of five Wave Dragon WECs, installed in a staggered grid, is studied.

4 A farm of 5 Wave Dragon WECs

The power absorption of one Wave Dragon WEC affects the available wave power for the Wave Dragon WECs in its lee. The reduction of the available wave power depends on the distances between the Wave Dragon WECs in a farm, on the incident wave climate (transmission under main body and wave reflectors increases for increasing wave period and wave height) and on the directional spreading of the incident waves. As a large distance between two Wave Dragon WECs, installed right behind each other, is needed to have an acceptable production of the second Wave Dragon WEC, the latter Wave Dragon WEC will be shifted, resulting in a staggered grid (Fig. 9).

A minimal lateral spacing w of 255 m is needed between two adjacent Wave Dragon WECs to prevent collision, as the movement of the Wave Dragon WEC is assumed to be restricted to ±60° by its anchor system [18]. In this section the power absorption of a farm of 5 Wave Dragon WECs installed in a staggered grid with varying lateral and longitudinal spacing will be studied for the wave situation with the highest frequency of occurrence (wave situation 1) and a wave situation with a higher contribution to the yearly power absorption of the Wave Dragon (wave situation 3)(Table 1).

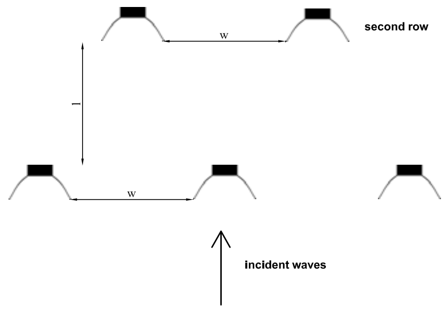

Figure 9: 5 Wave Dragon WECs with a lateral spacing w and a longitudinal spacing l installed in a staggered grid

The wave height reduction behind a row with 3 Wave Dragon WECs with a lateral spacing of D, $2D$ and $3D$, with D the distance between the tips of the wave reflectors of a single WEC (= 260 m), is shown in Fig. 10 for wave situation 1 with a directional spreading of 24° ($s_{max} = 10$), in Fig. 11 for wave situation 3 with a directional spreading of 9° ($s_{max} = 75$) and in Fig. 12 for wave situation 3 with a directional spreading of 24° ($s_{max} = 10$). Again only the useful domain without sponge layers is shown. For wave situation 1 and 3 each Wave Dragon WEC is absorbing $P_{cs,B,a} = U$. It is clear that more energy is travelling in-between the WECs when the lateral spacing is increasing and the directional spreading is decreasing (Fig. 11). The wake behind a row of Wave Dragon WECs is a little smaller and shorter for wave situation 3 (Fig. 12) compared to wave situation 1 (Fig. 10) as the transmission under the main body and wave reflectors is higher for wave situation 3. Furthermore the wave height decrease immediately behind the WECs is higher for wave situation 1. When K_d = 0.85, 0.9 and 0.95 the potential power absorption is 0.66 U, 0.77 U and 0.88 U (Eqn. (7)), respectively. The power absorption is very fast decreasing when the wave height is decreasing. It seems more reasonable to install a second row of Wave Dragon WECS as close as possible to the first row in stead of placing them further away, as even in the case with the highest energy transmission and refill behind the first row of WECs (Fig. 12(c)) a distance of approximately 2 km is needed to have a sufficient high value of K_d.

A minimal longitudinal spacing l of 190 m, 130 m and 0 m is needed between two adjacent Wave Dragon WECs to prevent collision when the lateral spacing is D, $2D$ and $3D$, respectively. The positions of Wave Dragon WECs in the second row are indicated on Fig. 10, Fig. 11 and Fig. 12.

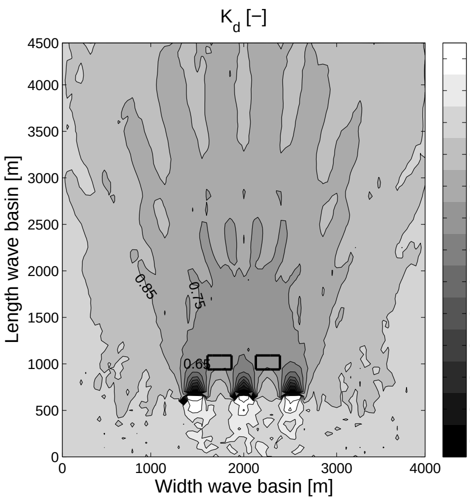

(a) lateral spacing of D

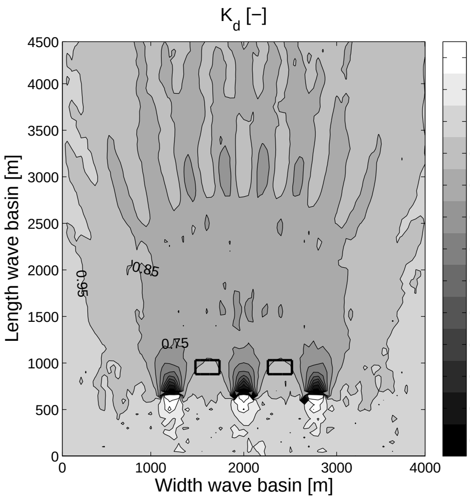

(b) lateral spacing of 2D

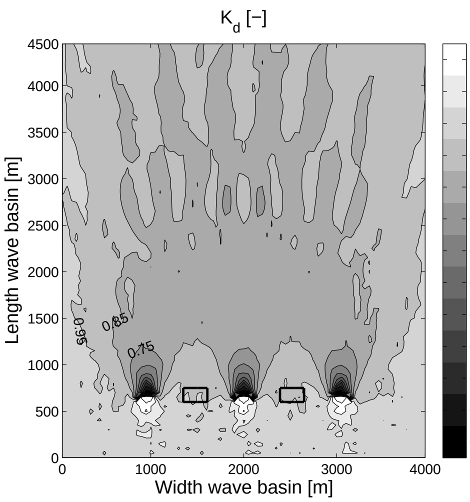

(c) lateral spacing of 3D

Figure 10: Calculated disturbance coefficient K_d in a wave basin with 3 Wave Dragon WECs with a lateral spacing of (a) *D*, (b) 2*D* and (c) 3*D*, for short-crested waves (SCW) with T_p = 5.6 s (wave situation 1) and s_{max} = 10

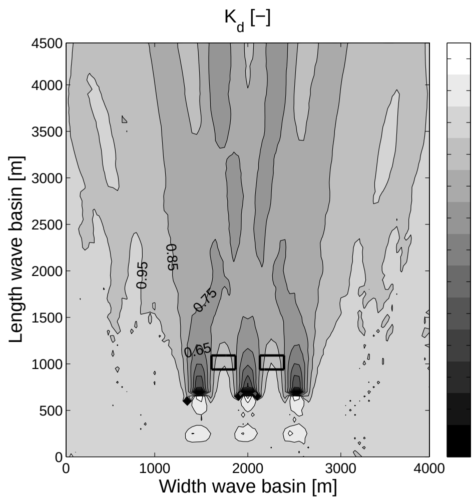

(a) lateral spacing of D

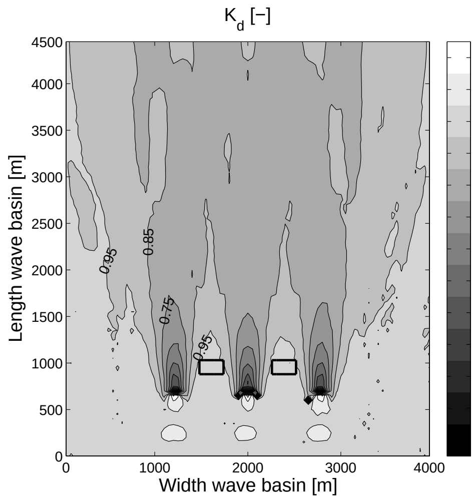

(b) lateral spacing of 2D

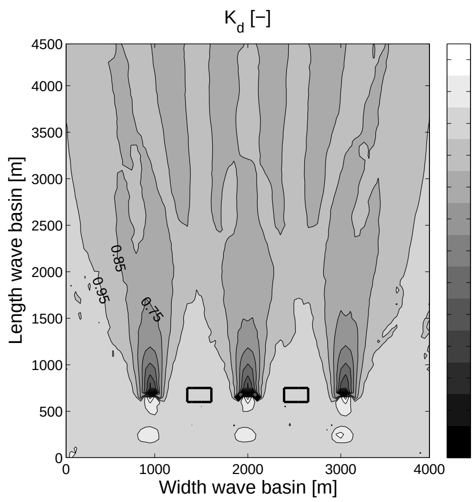

(c) lateral spacing of 3D

Figure 11: Calculated disturbance coefficient K_d in a wave basin with 3 Wave Dragon WECs with a lateral spacing of (a) *D*, (b) 2*D* and (c) 3*D*, for short-crested waves (SCW) with T_p = 8.4 s (wave situation 3) and s_{max} = 75

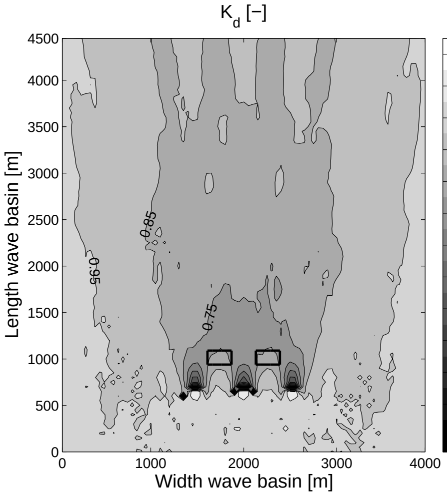

(a) lateral spacing of D

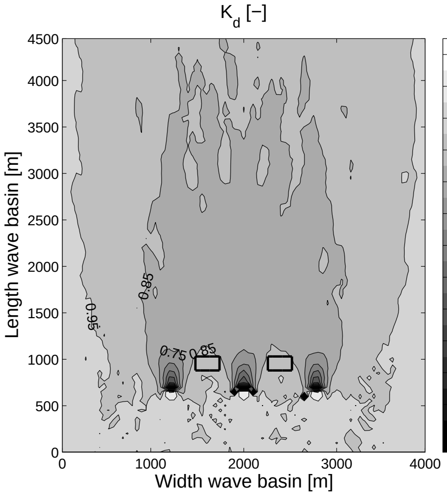

(b) lateral spacing of 2D

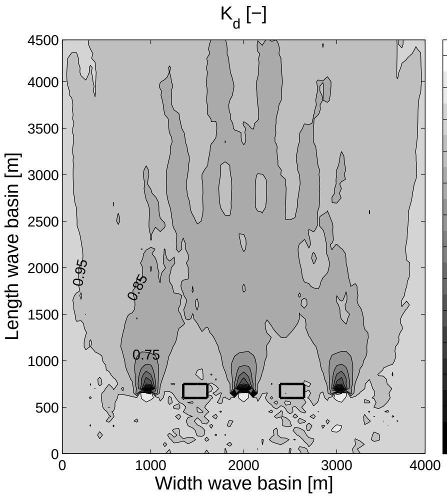

(c) lateral spacing of 3D

Figure 12: Calculated disturbance coefficient K_d in a wave basin with 3 Wave Dragon WECs with a lateral spacing of (a) *D*, (b) 2*D* and (c) 3*D*, for short-crested waves (SCW) with T_p = 8.4 s (wave situation 3) and s_{max} = 10

The loss of the amount of absorbed power of the farm compared to the power absorption of a theoretical farm of five independent Wave Dragon WECs (= 5*U*) is given in Table 2.

Table 2: Power absorption of a farm of 5 Wave Dragon WECs

Wave situation [−]	*w* [multiple of D]	σ [°]	Loss of power absorption [multiple of U]
1	1	24	1.09
1	2	24	0.42
1	3	24	0
3	1	9	0.46
3	2	9	0.10
3	3	9	0
3	1	24	0.88
3	2	24	0.35
3	3	24	0

The power loss of a farm for wave situation 1 is a little higher compared to wave situation 3 (directional spreading of 24° - $s_{max} = 10$). Furthermore more energy is absorbed in a wave condition with a smaller directional spreading because more energy is travelling in-between the WECs. For a lateral spacing of *D* and a directional spreading of 24° ($s_{max} = 10$) five Wave Dragon WECs are absorbing approximately the same as four single Wave Dragon WECs. In the latter case Wave Dragon WECs in the second row are only absorbing half of the power absorbed by a Wave Dragon WEC in the first row. For a lateral spacing of 3*D*, the WECs of the second row are placed in-between the WECs of the first row, resulting in a single row of five Wave Dragon WECs with a lateral spacing of *D*. Each WEC is absorbing the same amount of power as a single WEC.

Not only the amount of absorbed power is important when comparing several lay-outs, but also the use of available sea area and the cost of the cabling in the farm need to be taken into account. To make a better comparison between the considered lay-outs, the power absorption per km^2 and the power absorption per *km* are studied. When calculating the power absorption per km^2 an area with half of the lateral spacing, respectively, longitudinal spacing has been added at the right and left end of the farm, respectively, in front of and behind the farm. By dividing the amount of absorbed power by the width of the farm (including half of the lateral spacing at both ends), the power absorption per *km* is obtained. The results are shown in Table 3. The absorption for wave situation 1 is smaller compared to wave situation 3 as the incident wave power is smaller as well (Table 1). Therefore the farm efficiency (= ratio between power absorption per *km* and incident wave power (Table 1)) is calculated as well. The difference in farm efficiency between wave situation 1 and 3 is very small.

Table 3: Power absorption per km^2 and per km

Wave situation	w	σ	Power absorption per km^2	Power absorption per km	Farm efficiency
$[-]$	[D]	[°]	$[MW/km^2]$	$[MW/km]$	[%]
1	1	24	0.6	0.3	13
1	2	24	0.5	0.2	10
1	3	24	1.6	0.2	10
3	1	9	8.2	4.7	14
3	2	9	7.2	3.4	10
3	3	9	20.6	3.1	9
3	1	24	7.5	4.2	13
3	2	24	6.8	3.2	10
3	3	24	20.6	3.1	9

Five Wave Dragon WECs installed in a single row with a lateral spacing of D results in the highest energy absorption per km^2. On the other hand the absorption per km is lower compared to a farm of five Wave Dragon WECs installed in two rows. To produce a considerable amount of wave power more than 50 Wave Dragon WECs need to be installed in a farm. When all Wave Dragon WECs are installed in a single row with a lateral spacing of D a width of more than 25 km is needed. In practice an available space with a width of 25 km is rather scarce. Furthermore the cost of cabling inside the farm will increase. A farm of five Wave Dragon WECs with $w = D$ and l = 190 m results in a higher absorption per km^2 and per km compared to a farm with w = 2D and l = 130 m. Furthermore to install 50 Wave Dragon WECs a width of only 13 km is needed. On the other hand the power loss is twice as high compared to a farm with w = 2D and l= 130 m. When short-crested waves with a small directional spreading occur, the power loss is very small for a staggered grid with w = 2D and l = 130.

Consequently the staggered grid with w = 2D and l = 130 m seems to be the best option. Furthermore in this case the width of a farm of 50 Wave Dragon WECs is reduced with 25 % compared to a single row of Wave Dragon WECs. Note that in this study only head-on waves have been considered. The power absorption will decrease when other main wave directions are taken into account.

It is clear that a single row or two rows of Wave Dragon WECs are absorbing a lot of energy. Consequently the transmission is rather low. In all cases the wave height 3 km behind a single row of Wave Dragon WECs is at minimum 15 % lower than the wave height in front of the farm. Installing a row of Wave Dragon WECs in front of a farm of windturbines will facilitate the maintenance of the windturbines as the wave height is lower. The latter effect will even be higher when more than 1 row is installed. One should keep in mind that only two wave situations have been presented (wave situation 1 and 3). The transmission for wave situation 4 and 5 is slightly higher compared to wave situation 1 and 3. More energy will be available behind these WECs. On the other hand these wave situations do not occur very often (Table 1).

To install more rows behind each other on a reasonable distance, more energy should be transmitted under the wave reflectors and main body. Decreasing the nominal power of the device (and consequently cost of the device) could be an option. A cost study is needed to check whether this option is feasable.

5 Conclusions

In this paper the wake effects in the lee of a single Wave Dragon WEC and a farm of Wave Dragon WECs have been studied in the time-dependent mild-slope equation model MILDwave. A Wave Dragon WEC has been implemented as a porous structure with the same reflection, absorption and transmission characteristics as obtained for the prototype by using the sponge layer technique.

The wake effects in the lee of a single Wave Dragon WEC have been calculated for the wave situation with the highest frequency of occurrence in a northern North Sea wave climate (24 kW/m). For irregular long-crested (head on) waves a large decrease of wave power is observed behind the Wave Dragon WEC. For short-crested waves a faster wave redistribution is observed. The available wave power 3 km behind the WEC is approximately equal to the incident wave power for short-crested waves with s_{max} = 10 (and H_s = 1 m, T_p = 5.6 s). When installing multiple WECs in a farm, the placing of a WEC in a second row right behind a WEC in the first row should be avoided. A staggered grid lay-out is preferred.

The power absorption of a farm of five Wave Dragon WECs installed in a staggered grid, with a lateral spacing of D, $2D$ and $3D$ (D = distance between the tips of the wave reflectors of a single WEC) and a longitudinal spacing of 190 m, 130 m and 0 m, respectively, has been modelled for the wave situation with the highest frequency of occurrence (H_s = 1 m and T_p = 5.6 s) and a wave situation with a high contribution to the yearly power absorption (H_s = 3 m and T_p = 8.4 s). A farm with $w = 2D$ and l = 130 m combines a relatively high power absorption with an acceptable farm width. The power absorption per km^2 is rather low.

The wave height decrease 3 km behind a single row of Wave Dragon WECs is at minimum 15 %. Installing a row of Wave Dragon WECs in front of a farm of windturbines could make the installation and maintenance of the windturbines easier.

Further research will focus on the ratio between the cost and the power absorption of a farm of Wave Dragon WECs.

Acknowledgements

Research funded by Ph.D. grant of the Institute for the Promotion of Innovation through Science and Technology in Flanders (IWT-Vlaanderen), Belgium.

The authors would like to thank Tom Versluys for his contribution in optimising the code and developing a graphical interface.

Thanks go to Robby Caspeele and Sam Pecqueur for their assistance in extending the wave generation technique.

Wave Dragon ApS. (WD-MW FP6 EU project) and James Tedd (Aalborg University) are gratefully acknowledged for providing the data on which this study is based.

References

[1] J. P. Kofoed, P. Frigaard, E. Friis-Madsen, and H. C. Sørensen. Prototype testing of the wave energy converter Wave Dragon. *Renewable energy*, 31:181–189, 2006.

[2] C. Beels, P. Troch, G. De Backer, J. De Rouck, T. Moan, and A. F. de O. Falcão. A model to investigate interacting wave power devices. In *Proceedings of the International Conference Ocean Engineering*, Bremerhaven, 2006.

[3] C. Beels, P. Troch, K. De Visch, J. P. Kofoed, and G. De Backer. Application of the time-dependent mild-slope equations for the simulation of wake effects in the lee of a farm of Wave Dragon wave energy converters. *Renewable energy*, Submitted for publication, 2009.

[4] A. C. Radder and M. W. Dingemans. Canonical equations for almost periodic, weakly nonlinear gravity waves. *Wave Motion*, 7:473–485, 1985.

[5] N. Booij. A note on the accuracy of the mild-slope equation. *Coastal Engineering*, 7:191–203, 1983.

[6] C. Lee and K. D. Suh. Internal generation of waves for time-dependent mild-slope equations. *Coastal Engineering*, 34:35–57, 1998.

[7] Z. Liu and P. Frigaard. Random seas. Technical report, Hydraulics and Coastal Engineering Laboratory, Aalborg University, 1997.

[8] C. Lee and S. B. Yoon. Internal generation of waves on an arc in a rectangular grid system. *Coastal Engineering*, 54:357–368, 2007.

[9] H. Mitsuyasu, F. Tasai, T. Suhara, S. Mizuno, M. Ohkusu, T. Honda, and K. Rikiishi. Observations of the directional spectrum of ocean waves using a cloverleaf buoy. *Journal of Physical Oceanography*, 5:750–760, 1975.

[10] Y. Goda and Y. Suzuki. Computation of refraction and diffraction of sea waves with mitsuyasu's directional spectrum. *Tech. Note of Port and Harbour Res. Inst.*, 230, 1975.

[11] J. Larsen and H. Dancy. Open boundaries in short wave simulations - a new approach. *Coastal Engineering*, 7:285–297, 1983.

[12] M. Brorsen and J. Helm-Petersen. On the reflection of short-crested waves in numerical models. In *Proceedings of the* 26^{th} *International Conference on Coastal Engineering*, Copenhagen, 1998.

[13] K. D. Suh, C. Lee, Y. H. Park, and T. H. Lee. Experimental verification of horizontal two-dimensional modified mild-slope equation model. *Coastal Engineering*, 44:1–12, 2001.

[14] K. Nielsen and M. Rugbjerg. Kortlægning af bølgeenergiforhold i den danske del af Nordsøen. Technical report, Rambøll, 1999.

[15] M. Kramer and P. Frigaard. Efficient wave energy amplification with wave reflectors. In *Proceedings of the* 9^{th} *ISOPE conference*, 2002.

[16] J. P. Kofoed. *Wave overtopping of marine structures - utilization of wave energy*. PhD thesis, Hydraulics and Coastal Engineering Laboratory, Department of Civil Engineering, Aalborg University, 2002.

[17] J. Tedd, J. P. Kofoed, W. Knapp, E. Friis-Madsen, and H. C. Sørensen. Wave Dragon prototype wave power production. In *Proceedings of the World Renewable Energy Congress - IX*, Florence, 2006.

[18] J. Tedd, J. P. Kofoed, E. Friis-Madsen, and L. Christensen. 7.5.5 Wave Dragon. In J. Cruz, editor, *Ocean wave energy, Current Status and Perspectives*, pages 371–382. Springer, 2008.